ACS APPLIED MATERIALS & INTERFACES

www.acsami.org

Research Article

Real-Time Alignment and Reorientation of Polymer Chains in Liquid Crystal Elastomers

Chaoqian Luo, Christopher Chung, Christopher M. Yakacki, Kevin Long,* and Kai Yu*

Cite This: *ACS Appl. Mater. Interfaces* 2022, 14, 1961−1972

Read Online

ACCESS | Metrics & More | Article Recommendations | Supporting Information

ABSTRACT: Liquid crystal elastomers (LCEs) exhibit soft elasticity due to the alignment and reorientation of mesogens upon mechanical loading, which provides additional mechanisms to absorb and dissipate energy. This enhanced response makes LCEs potentially transformative materials for biomedical devices, tissue replacements, and protective equipment. However, there is a critical knowledge gap in understanding the highly rate-dependent dissipative behaviors of LCEs due to the lack of real-time characterization techniques that probe the microscale network structure and link it to the mechanical deformation of LCEs. In this work, we employ in situ optical measurements to evaluate the alignment and reorientation degree of mesogens in LCEs. The data are correlated to the quantitative physical analysis using polarized Fourier-transform infrared spectroscopy. The time scale of mesogen alignment is determined at different strain levels and loading rates. The mesogen reorientation kinetics is characterized to establish its relationship with the macroscale tensile strain, and compared to theoretical predictions. Overall, this work provides the first detailed study on the time-dependent evolution of mesogen alignment and reorientation in deformed LCEs. It also provides an effective and more accessible approach for other researchers to investigate the structural-property relationships of different types of polymers.

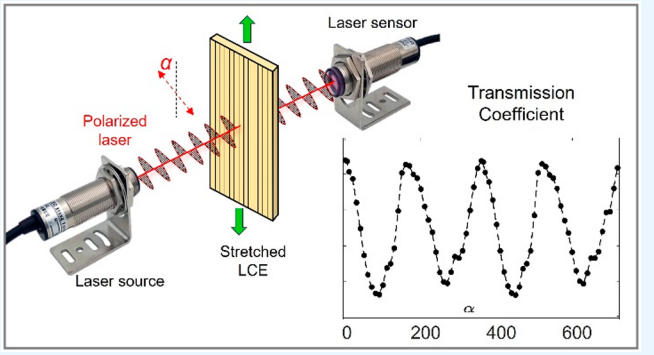

KEYWORDS: *Mesogen alignment, reorientation, polarized optimal measurements, Fourier-transform infrared spectroscopy, liquid crystal elastomer, real-time characterization*

1. INTRODUCTION

Liquid crystal elastomers (LCEs) exhibit unique mechanical properties of soft elasticity and enhanced energy dissipation with unusual rate dependence.[1,2] They show potential to be transformative materials for mechanical impact and vibration mitigation,[2−8] biomedical devices, tissue replacements, and protective equipment.[9−14]

The unique capabilities of LCEs originate from the organization of liquid crystal (LC) mesogens, which are rod-like aromatic structures (i.e., mesogens, usually 2−3 linked benzene rings) built into the polymer network.[15−22] When stretching a polydomain LCE, the LC mesogens gradually reorient and align themselves in the stretching direction. This process serves as a second mechanism to dissipate energy in addition to the viscoelastic relaxation of polymer chains. It provides LCEs with enhanced mechanical energy absorption and dissipation capabilities, the latter of which can potentially match the viscous behavior of a liquid.[1,2,15,18,23−28]

To understand the unusual and highly rate-dependent dissipative behaviors of LCEs, it is important to connect the state of mesogen alignment with the mechanical deformation in situ. Currently, wide-angle X-ray scattering (WAXS) is the most commonly adopted technique to characterize the microscale organizations of LC mesogens.[29−36] The diffraction patterns of X-ray intensity at different azimuthal angles can be used to determine the mesogen direction and alignment degree. However, a major limitation of WAXS is the low speed to acquire the diffraction pattern. Depending on the performance of employed X-ray detectors, a WAXS measurement typically takes more than 5 min to obtain the data of mesogen alignment degree,[29−33] which restricts the characterizations to near equilibrium (time-independent) material behavior. Therefore, this approach cannot be used to investigate material rate-dependent dissipative behavior, which remains a critical knowledge gap for the aforementioned applications.

Recently, polarized Fourier-transform infrared spectroscopy (FTIR) has been adopted to characterize the macromolecular structure of LCEs,[20,27,37−41] wherein each FTIR scan can be generated within one second to enable near real-time

Received: October 18, 2021
Accepted: December 8, 2021
Published: December 21, 2021

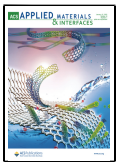

https://doi.org/10.1021/acsami.1c20082
ACS Appl. Mater. Interfaces 2022, 14, 1961−1972

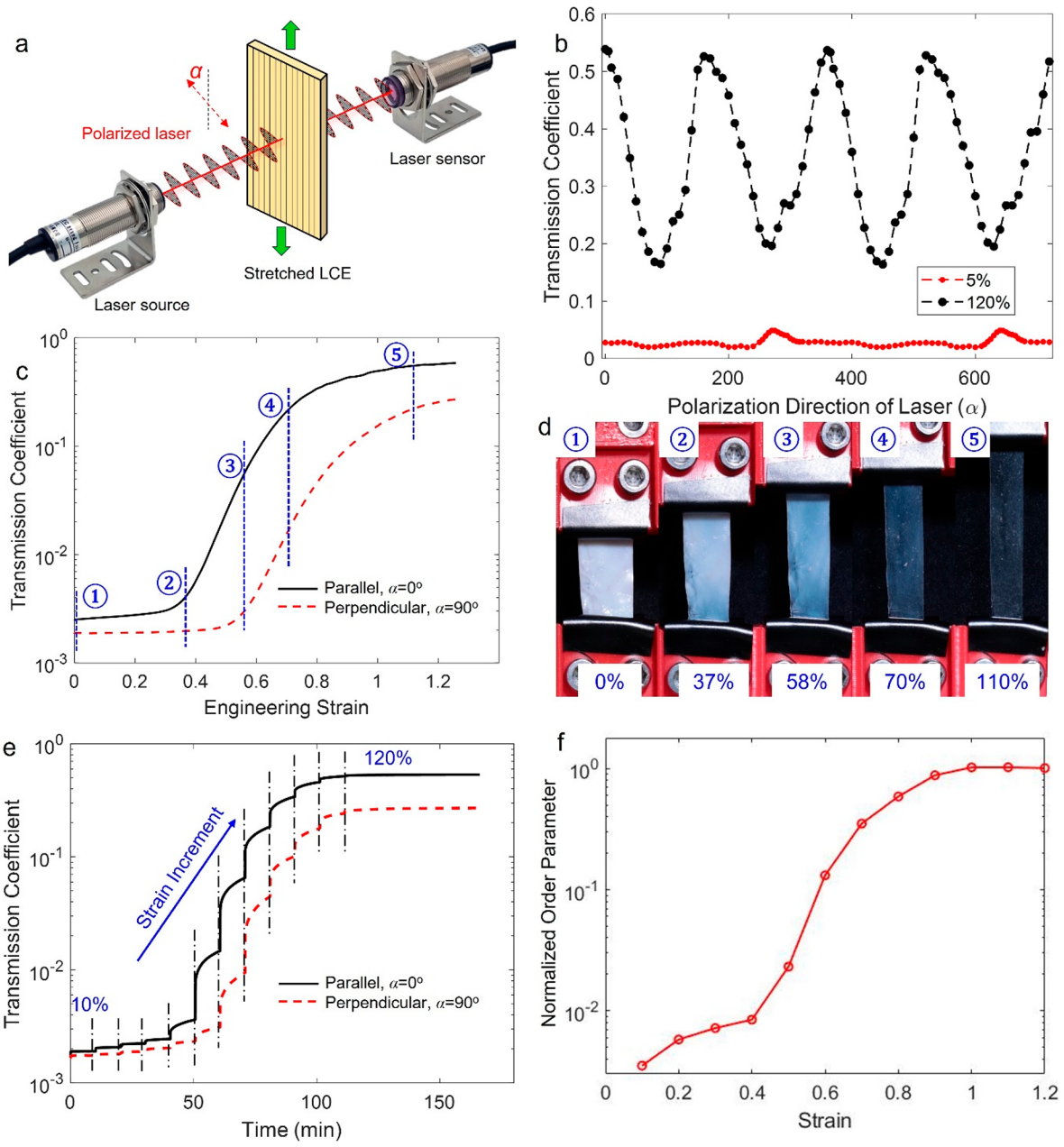

Figure 1. (a) Experimental setup to determine the transmission coefficient of polydomain LCE samples under tension. The angle between the light polarization and stretching direction is denoted as α. (b) The directional transmission coefficients of the polydomain LCE at different directional angles of polarized light. (c) Increment of the transmission coefficient of the polydomain LCE in both parallel and perpendicular directions of stretch. The LCE sample was stretched in a continuous manner (1%/min). (d) Appearances of the polydomain LCE samples under tension. (e) The transmission coefficient of the polydomain LCE in both parallel and perpendicular directions of stretch. The LCE sample was stretched in a stepped manner. (f) The evolution of mesogen order parameters with different strain levels.

characterizations. During the tests, LCE samples are exposed to polarized light. Chemical bonds (e.g., LC mesogens) on the chain backbone have the strongest light absorption when the nematic director state (corresponding to the average mesogen orientation) is parallel to the polarizer and the weakest absorption when perpendicular. Their alignment degree can be identified by comparing the absorption peaks at different irradiation directions. While the FTIR characterization is much faster than WAXS, it requires specific functional groups built on the chain backbone, which have absorption peaks that are distinguishable on the FTIR spectrum.

Compared to the FTIR analysis, cross-polarized optical measurements can provide even faster data collection controlled by the output frequency of the light power meter and the data acquisition process. This faster measurement enables the in situ characterizations on the highly rate-dependent behaviors of LCEs. This technique does not require special chemical compositions of the LCE sample (beyond the obvious requirement that the network forms a nematic or other LC phase). Previous studies show that stretched LCEs with highly aligned polymer chains show distinguished refractive indexes in the directions perpendicular and parallel to the alignment direction. The differences in the refractive index can

https://doi.org/10.1021/acsami.1c20082
ACS Appl. Mater. Interfaces 2022, 14, 1961−1972

be used to estimate the network anisotropy and mesogen alignment degree.[16] While many studies investigate network equilibrium at different temperatures and strain,[42−47] the transient response concerning mechanical deformations at different loading rates has not been adequately explored. In addition, the estimations of the mesogen alignment and orientation are usually presented qualitatively without connection to the quantitative WAXS or FTIR characterizations on the state of mesogens.

This paper examines the rate-dependent mesogen alignment and reorientation of nematic LCEs in situ using polarized optical and FTIR measurements. A correlation in mesogen alignment degree between these two characterization techniques is first established. It is used to determine the time scale of the mesogen alignment of polydomain LCE samples at different strain levels and loading rates. Then, the mesogen reorientation is characterized by stretching a monodomain LCE sample in an oblique direction of the mesogen orientation. The relationship between the macroscale tensile strain and microscale mesogen direction is revealed and compared to theoretical predictions. Overall, this work provides the first detailed study on the real-time evolution of mesogen alignment and reorientation in deformed LCE networks, which is critical to understand their unusual mechanical behavior and assist in their application deployment. The approach also provides an effective and more accessible approach for other researchers to investigate the structural-property relationships of different types of polymeric materials that have polarizing molecular functionalities.

2. RESULTS AND DISCUSSION

2.1. Optical Properties and Mesogen Alignment Degree of Polydomain LCE Networks. Polydomain LCE samples were synthesized using the thiol−acrylate Michael addition (see the Materials and Methods for details). The experimental setup to characterize the optical properties of stretched polydomain LCE is illustrated in Figure 1a. The sample with a 1.1 mm initial thickness was stretched to 5% and 120% engineering strain respectively at 1%/min and then stabilized for 30 min. Due to the slow loading rate and extended stabilization period, the LCE samples after stretching were in the equilibrium state without notable stress relaxation. Their optical properties and microscale network structures were expected to be maintained during the subsequent tests.

A linearly polarized visible light (650 nm wavelength) with an incident power of $T_0 = 18.24 \times 10^{-5}$ W was then irradiated on the center position of the sample with different directional angles between the light polarization and stretching direction. The power of the transmitted light, T, was measured using a light sensor. As shown in Figure 1b, at a low strain level of 5%, the transmission coefficient of the LCE sample, T/T_0, is near identical in different directions of stretch. When the strain is increased to 120%, the transmission coefficient strongly depends on the directional angle. The stretched LCEs with highly aligned mesogens behave like a light polarizer. Therefore, the transmission coefficient is the highest when the light polarization is parallel to the stretching direction and the lowest when it is perpendicular to the stretching direction.

In the Supporting Information (SI, Section S1), the transmission coefficients of stretched LCE at different polarization directional angles are compared to control samples without mesogens on the chain backbone. The strain and incident light power were set to be the same. It is observed that there are some variations in the transmission coefficients of control samples when the orientation of light polarization is changed. However, the peak-to-valley intensity is much lower than that of the LCE sample. Therefore, the alignment of the polymer backbones causes negligible influences on the overall anisotropy of the LCE network. The directional optical measurement results of LCE samples in Figure 1b are mainly showing the effects of LCE mesogen alignment and not just polymer chains.

A polydomain LCE sample was stretched continuously at 1%/min to 120% engineering strain. The evolution of the transmission coefficients in the parallel and perpendicular stretch directions was monitored and shown in Figure 1c. They are observed to increase with the strain at different time scales. For example, when the light polarization is parallel direction of stretching, the transmitted light power dramatically increases at ∼37% strain and saturates at ∼90%. With the light polarization oriented perpendicular to the loading direction, no notable change in transmitted power is observed until the strain reaches ∼58%. The appearances of the polydomain LCE samples during the stretch are shown in Figure 1d. The sample remains mostly opaque until the perpendicular transmission coefficient starts to increase. Because the polydomain LCE is transformed from the opaque to the transparent state after stretching, the perpendicular transmission coefficient increases with the strain, even though the aligned polymer chains tend to filter some light waves in the perpendicular direction.

The mesogen alignment degree within the polydomain LCE networks was examined under the stepped-loading condition. The LCE sample was stretched by 10% engineering strain within one second and then stabilized for 10 min to reach a near-equilibrium state. After that, the sample was stretched by another 10% to reach the next strain level. Figure 1e shows the evolution of transmission coefficients in the parallel and perpendicular directions of stretch. It is seen that within each loading step, the transmitted light power first increases instantaneously to some extent and then increases with time during the stabilization period, which suggests the time-dependent evolution of mesogen alignment degree. When the strain level is above ∼90%, the increment of light power is less notable, indicating that the chains are maximally extended and aligned in the stretching direction.

The transmission coefficients of LCE networks in the parallel and perpendicular directions of stretch are used to calculate the respective refractive index, which can be used to determine the order parameter of mesogen alignment S_L ($0 < S_L < 1$, a larger S_L suggests a higher level of alignment).[16] Since the light power attenuates along the thickness direction of LCE samples, the thickness change during the mechanical loading should be considered to calibrate the measured transmission coefficients of LCE networks. It is confirmed in the SI (Section S2) that the influence of the sample thickness on the transmission coefficient of LCE networks follows the well-known Beer's Law,[48−50] wherein the transmission coefficient scales to $\exp(-\beta t)$, with t being the sample thickness and β being the absorption coefficient depending on the material composition. In our experiment, when the LCE sample is stretched to the strain of $\varepsilon = 120\%$, the change in sample thickness is $1/\sqrt{(1+\varepsilon)} = 32.6\%$ under the assumption of incompressibility. This change in thickness influences the transmitted light power. To address this issue, we define the calibrated light power transmission, $T' = T^{1/\sqrt{(1+\varepsilon)}}$, with T

https://doi.org/10.1021/acsami.1c20082
ACS Appl. Mater. Interfaces 2022, 14, 1961−1972

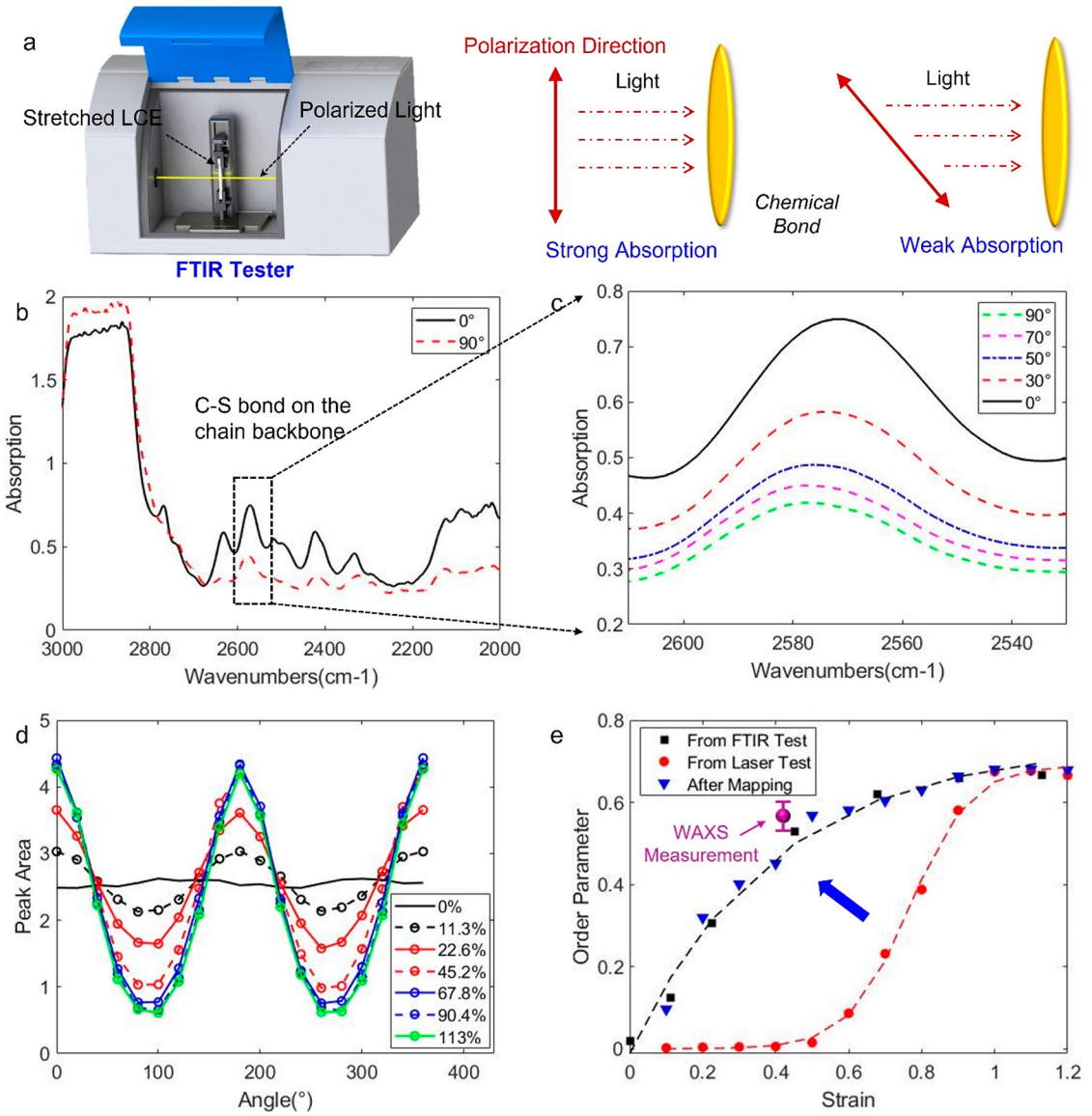

Figure 2. (a) Schematical view of the polarized FTIR characterizations. The LCE sample is stretched in the perpendicular direction. Polarized infrared light is shined through the sample center. (b) Two representative FTIR spectra of the LCE sample after being stretched to 113% strain. (c) The absorption peak of the C−S bond on the chain backbone with different directional angles of the polarized light. (d) Summary of the absorption peak areas of the C−S bond with different strain and polarization directions. (e) The evolution of the order parameter is determined using the FTIR, which is compared to those determined in the optical measurements.

being the transmitted light power in experiments. T' essentially represents the transmitted light power of LCE samples with the same mesogen alignment degree as the deformed sample but with unchanged thickness.

Note that during the optical measurements, the incident laser dot was small (~1 mm diameter) and was always at the center of the sample. Therefore, the decrease of sample width during the uniaxial tension tests did not affect the measurements.

According to Fresnel's equation,[51] when the incident light is normal to the sample surface, the transmission coefficient is related to the reflective index as below:

$$\frac{T'}{T_0} = \frac{4m_1m_2}{(m_1 + m_2)^2} \quad (1)$$

where $m_1 = 1$ is the refractive index of the air. m_2 is the refractive index of the LCE sample. Measuring the transmission coefficient in parallel and perpendicular directions obtains the refractive indices, respectively. The difference in refractive index in these two directions,

$$\Delta m_2 = m_{2//} - m_{2\perp} \quad (2)$$

is used to determine the order parameter $S_L = \Delta m_2/\Delta m_{20}$.[16] The normalization parameter, Δm_{20}, describes the intrinsic anisotropy of the network. It depends on the molecular factors and can be taken as the value Δm_2 at high strain levels when the mesogens are maximally aligned.

The determined order parameters at the end of each loading step are plotted in Figure 1f as a function of strain. It is observed to notably increase at about the same strain level as the parallel transmission coefficient and saturates at ~90%. In the SI, the order parameters of thicker LCE samples (1.7 mm and 3.9 mm thickness) were characterized using the same method, which show a similar evolution as the thinner sample

https://doi.org/10.1021/acsami.1c20082
ACS Appl. Mater. Interfaces 2022, 14, 1961−1972

(1.1 mm thickness) investigated in this section. Since the transmission coefficient and refractive indexes are both normalized, the sample thickness therefore has negligible influence on the optical measurements of mesogen alignment degree.

2.2. Calibration of Mesogen Alignment Degree of Polydomain LCEs with FTIR Analysis. The mesogen order parameter presented in Figure 1e has two pitfalls. First, since the refractive index at the highest strain level is taken as the normalizer in eq 2, the mesogen order parameter at the highest strain level is one, which means all the mesogens are perfectly aligned. However, perfect alignment is not physically realizable in the LCE networks. Second, the mesogen order parameter is lower than that tested using WAXS or FTIR at the smaller strain levels. For example, previous WAXS studies suggest a ~0.55 order parameter when the strain level is 40%.[29] The notable difference between optical, FTIR, and WAXS measurements is due to their different working mechanisms. The physical FTIR or WAXS analysis examines the alignment degree of a specific functional group (e.g., mesogens) on the chain backbone. In contrast, the macroscopic optical measurements interrogate the overall chain alignment degree (averaged over all functional groups) based on the transmission coefficients of polarized light. Therefore, the alignment degree determined by the optical measurements is seen to be lower than that in the FTIR analysis, especially at lower strain levels. To this end, the mesogen alignment in the LCE samples was tested using polarized FTIR analysis to calibrate the optical measurement results.

A polydomain LCE sample was first stretched by 113% engineering strain and stabilized for 30 min to be subject to the polarized FTIR tests (Figure 2a). Two representative absorbance spectra are shown in Figure 2b, where the polarizer of infrared light is parallel ($\alpha = 0°$) and perpendicular ($\alpha = 90°$) to the stretching direction. Conventionally, the C−H groups in aromatic rings, which have a distinguishable absorption peak at 3300−3350 cm^{-1}, can be used as an ideal signature to determine the alignment of mesogens. However, due to the potential presence of moisture in the LCE network, this absorption peak is diluted and hard to be detected in the FTIR spectra. Here, we chose to examine the absorption of C−S groups at ~2630 cm^{-1}, which was in the polymer backbone and indicative of the alignment of the polymer chains. Since the alignment of the polymer chains and the mesogen units are inherently linked, this peak was used to characterize the sample alignment.

Note that in addition to the highlighted C−S group at ~2630 cm^{-1}, there are other absorption peaks nearby, which might be related to the C−O bond on the chain backbone, C═O of the ester bonds, the unreacted C═C, respectively. These absorption peaks are all seen to be maximum when the polarizer of infrared light is parallel to the stretching direction and be minimum when they are perpendicular, which suggests that these chemical bonds could also be used as the reference to calibrate the optical measurement results. From this point of view, the presented characterization method may not be dramatically limited by the material composition.

The absorption peaks of the C−S bond within the stretched LCE network are shown in Figure 2c at different polarization directions of infrared light (from 0° to 90°). It is observed that when the polarization direction changes from perpendicular to parallel of the stretching direction, the height and area of the absorption peak both increases. Specifically, the peak area is seen to be increased by over eight times. The differences in the absorption peaks highly depend on the network strain. Herein, FTIR tests were repeated with different strain levels of the polydomain LCE samples, and the peak areas are plotted in Figure 2d as a function of polarization angle. When the LCE sample is stretched into an anisotropic network, the absorption peak area varies notably with polarization angle, showing a periodic pattern in terms of the polarization angle. The difference in the absorption peak and valley decreases at a lower strain level. For comparison, the absorbance of the control sample without deformation is plotted in the same figure, which shows a uniform absorbance independent of polarization direction.

The peak areas of the C−S bond in the parallel and perpendicular directions of stretch are used to calculate the dichroic ratio of the anisotropic LCE network: $D = A_{max}/A_{min}$, where A_{max} is the maximum absorbance in the parallel direction, and A_{min} is the minimum absorbance in the perpendicular direction. The order parameter S_F is determined as $S_F = (D - 1)/(D + 2)$.[41] The determined order parameters are plotted in Figure 2e (black square dots), which show an exponential increment as a function of strain level. The highest order parameter, ~0.66, is reached when the strain is above 90%. Note that the final order parameter at high strain levels depends on the cross-linking density of the LCE network. For example, in the SI (Section S3), a polydomain LCE network was synthesized with a lower cross-linking density than the network studied in this section. Using the polarized FTIR tests, the highest order parameter was determined to be ~0.73.

The mesogen order parameter of the thiol−acrylate LCE sample determined using WAXS measurement is also plotted in Figure 2e.[29] At ~40% engineering strain, the ~0.55 order parameter is close to the value determined using the FTIR measurements (~0.47). Even so, more WAXS measurements are needed in future work to find the quantitative relationship between the alignment degree of C−S bonds and mesogens on the chain backbone. In this study, the primary goal is to establish a strong correlation between the optical polarized microscopy and the microscale polarized FTIR analysis, which is sufficient to identify the kinetics of chain alignment and reorientation of LCE networks with different strain levels.

The order parameters obtained from the polarized optical measurements are presented for comparison (red circular dots). The maximum order parameter is normalized by the maximum value identified using the FTIR. It is observed that the increments of the order parameter in these two characterization techniques are significantly different, especially at the lower strain levels. To probe their quantitative relationships, a nonlinear regression method was used in MATLAB to determine the mathematical mapping between the order parameters determined in the FTIR analysis, S_F, and those determined in the optical measurement, S_L:

$$S_F = \alpha_1 e^{\beta_1 S_L} - \alpha_2 e^{\beta_2 S_L} \quad (3)$$

where the fitting parameters $\alpha_1 = 0.59$, $\beta_1 = 0.17$, $\alpha_2 = 0.59$, and $\beta_2 = -188.3$. Using this relationship, the order parameters determined in the optical measurements are mapped to the FTIR regime (blue triangular dots) in Figure 2e, which are shown to be nearly identical to the FTIR characterization results.

Note that the correlation in eq 3 is purely empirical without physical interpretation. The purpose is to establish a mathematical relationship between FTIR and optical measure-

https://doi.org/10.1021/acsami.1c20082
ACS Appl. Mater. Interfaces 2022, 14, 1961−1972

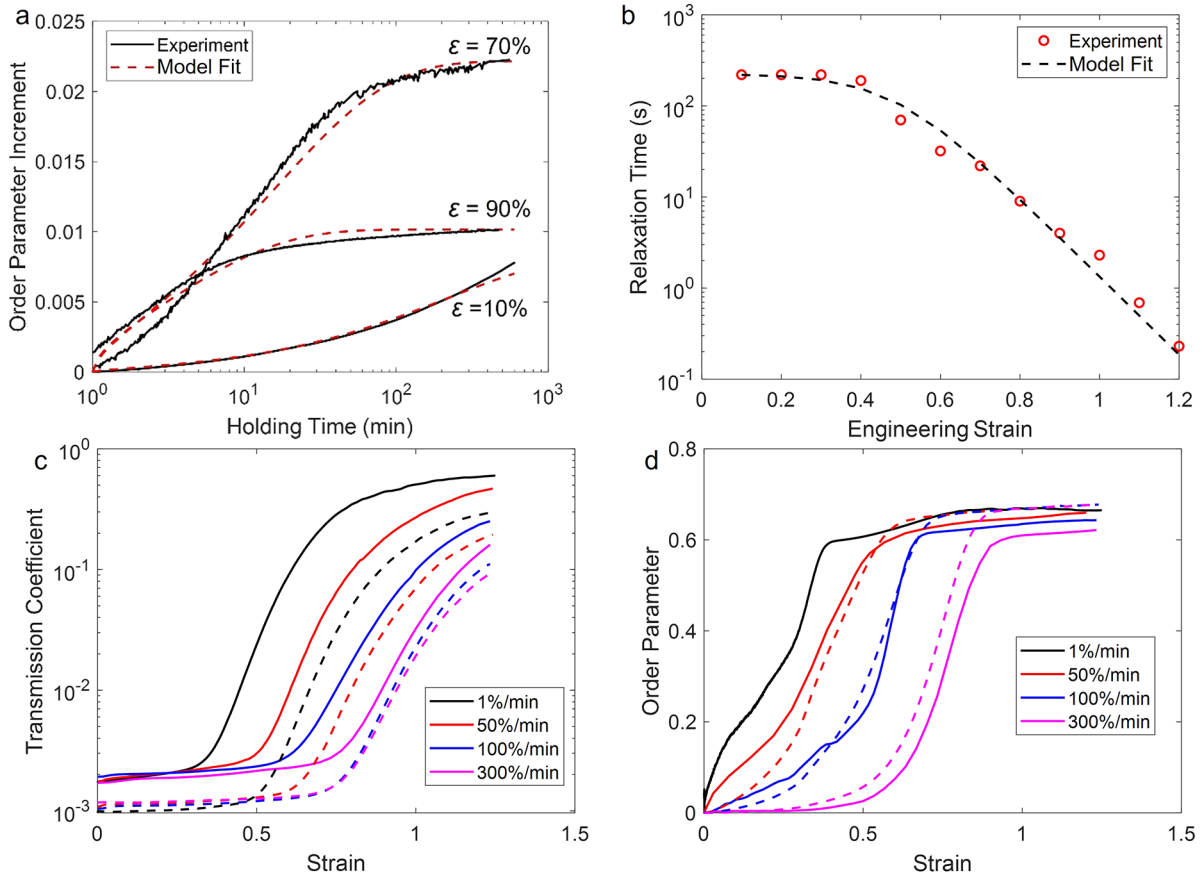

Figure 3. (a) Increment of mesogen order parameter during the stabilization period at 10%, 70%, and 90%, respectively, and associated model fits. (b) The relaxation times of the mesogen order parameter plotted as a function of strain. (c) The measured evolution of transmission coefficient when the LCE samples were stretched continuously to 120% at different strain rates. Solid lines: transmission coefficient in parallel direction of stretch. Dashed lines: perpendicular direction. (d) Evolution of the mesogen order parameters when the LCE samples were stretched continuously to 120%. Solid lines: experimental data. Dashed lines: Predictions after mapping the 1%/min curve.

ment results and reveal the time scale of chain alignment and reorientation within the LCE networks, which have been ignored in most existing works. The mapping equation may adopt a distinguished expression and coefficients when using the demonstrated method to characterize other types of polymers. A universal mapping equation might exist based on the working mechanisms between the FTIR and optical measurements, which is an interesting topic that deserves future rigorous study.

2.3. Rate-Dependency of the Mesogen Alignment in Polydomain LCE Networks. Using eq 3, one can probe the mesogen alignment degree of polydomain LCEs using the in situ optical measurements, and the testing results match those determined by the physical FTIR tests. To characterize the time scale of the rate-dependent evolution of mesogen order parameters, the optical measurement results with stepped loading conditions (Figure 1e) are re-examined. The evolution of order parameters is calculated based on the transmission coefficient (SI Figure S5) and then mapped using eq 3. The order parameters in each stabilization step are extracted to evaluate their time-dependent evolutions.

Figure 3a shows the evolution of order parameters when the strain level is 10%, 70%, and 90%, respectively. It is observed that the change of the order parameter over the whole stabilization period is the lowest at 10% strain. The net change in order parameter is three times higher when the strain is increased to 70%. The net change of order parameter at 90% strain is observed to be lower than that at 70% strain. This is because, at a higher strain level of 90%, the mesogens within the LCE networks have already been substantially aligned. Further increasing the strain does not dramatically increase the overall order parameter compared to that at a lower strain level. This can also be visualized in Figure 1e with the stepped loading condition. The change in the order parameter over the stabilization period is observed to be faster at intermediate and higher strain levels.

To characterize and model the time evolution of the order parameter at a fixed strain, we assume that there is a dominant time scale, τ, that determines the rate that the order parameter evolves toward its equilibrium value and that this rate is proportional to how far away from equilibrium the order parameter is[52,53]

$$\frac{dS}{dt'} = \frac{1}{\tau'}(S_{eq} - S) \tag{4}$$

wherein S_{eq} is the equilibrium order parameter at that strain. $\tau' = \tau^{\beta}$ and $dt' = \beta t^{\beta-1} dt$, t and τ are the physical time and relaxation time. Note that eq 4 uses a stretched exponential coefficient ($\beta = 0.65$) to stretch the relaxation time scale because real polymers typically exhibit distributed relaxation times.[54−57] Using the stretched exponential function greatly improves the predictions with respect to the experimental data. By fitting with the model predictions (dashed lines in Figure 3a) with the experimental data, the relaxation time τ at a

https://doi.org/10.1021/acsami.1c20082
ACS Appl. Mater. Interfaces 2022, 14, 1961−1972

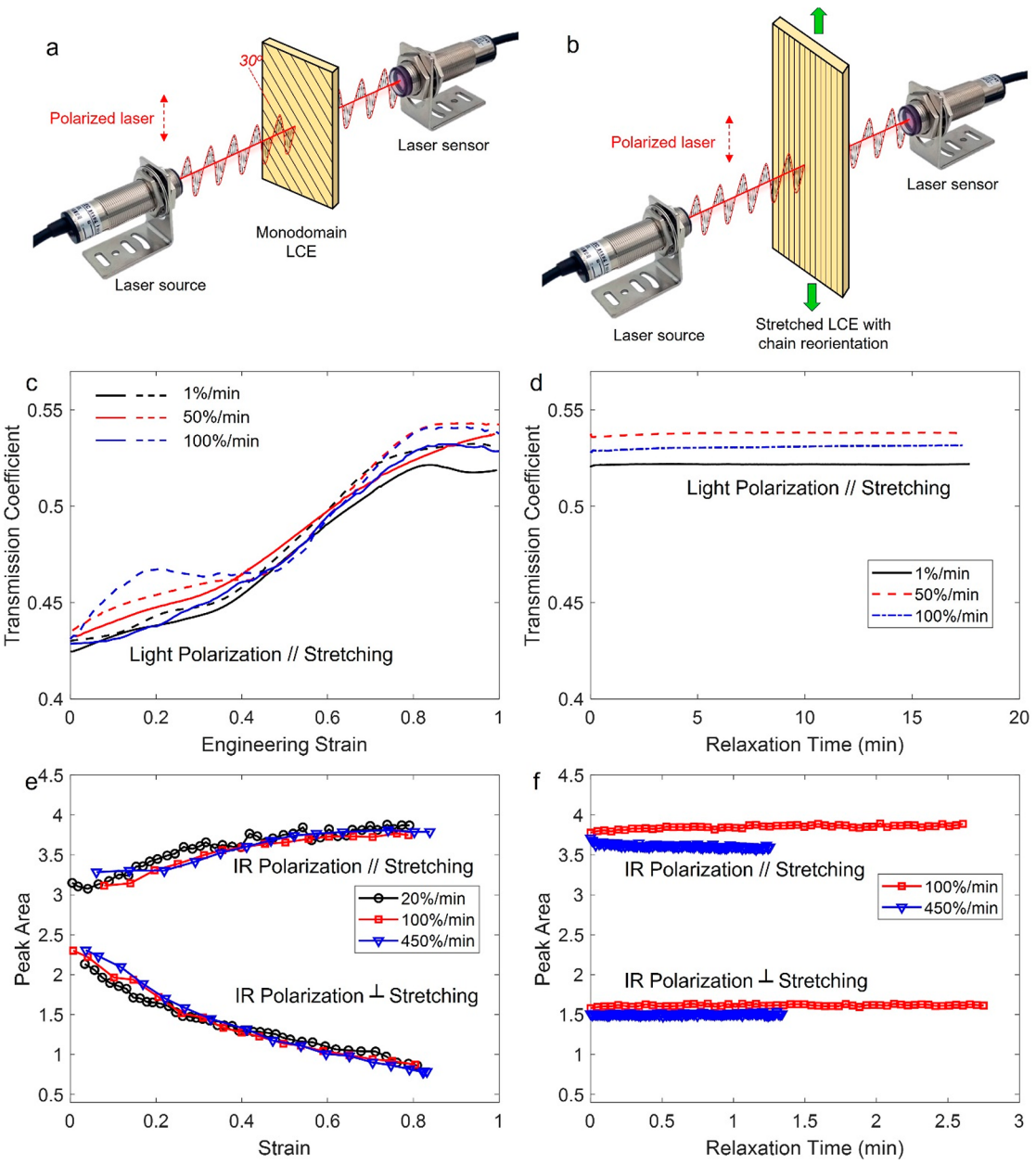

Figure 4. (a) The experimental setup to characterize the mesogen reorientation in the monodomain LCE. The initial mesogen direction is 30° with respect to the stretching direction. (b) The mesogen gradually aligned toward the tension direction when stretching the LCE sample in the perpendicular direction. (c) Increment of transmission coefficient when the monodomain LCE is continuously stretched at different loading rates. (d) The transmission coefficient during the subsequent stabilization step. (e) The evolution of absorption peak area during the FTIR measurements, wherein the LCE is continuously stretched at different loading rates. (f) The absorption peak area during the subsequent stabilization step.

specific strain level can be determined. The comparison between predictions and experimental data for all strain levels is shown in Figure S6 (SI).

The relaxation time of the order parameter is summarized in Figure 3b as a function of strain level. It is observed that the relaxation time is nearly a constant ~220 s when the strain is below 40% and then starts to decrease dramatically. This is because the force in each polymer chain at higher strain levels will be higher, which drives the reorientation and alignment of mesogens faster. Mathematically, the relationship between the relaxation times and strain levels can be regressed using the following empirical equation (dashed lines in Figure 3b):

$$\tau = \frac{a_1}{a_2 + e^{a_3 \varepsilon}} \tag{5}$$

wherein ε is the axial engineering strain. The fitting parameters $a_1 = 2.7 \times 10^3$ s, $a_2 = 120.8$, and $a_3 = 9.91$.

To further verify the evolution rule and relaxation times of the mesogen order parameter, the LCE sample was continuously stretched to 120% strain at different loading rates (1%/min, 50%/min, 100%/min, and 200%/min, respectively). The transmission coefficients were monitored in both parallel and perpendicular directions (Figure 3c). They are used to determine the evolution of order parameters within the LCE networks using the above-mentioned mapping

https://doi.org/10.1021/acsami.1c20082
ACS Appl. Mater. Interfaces 2022, 14, 1961−1972

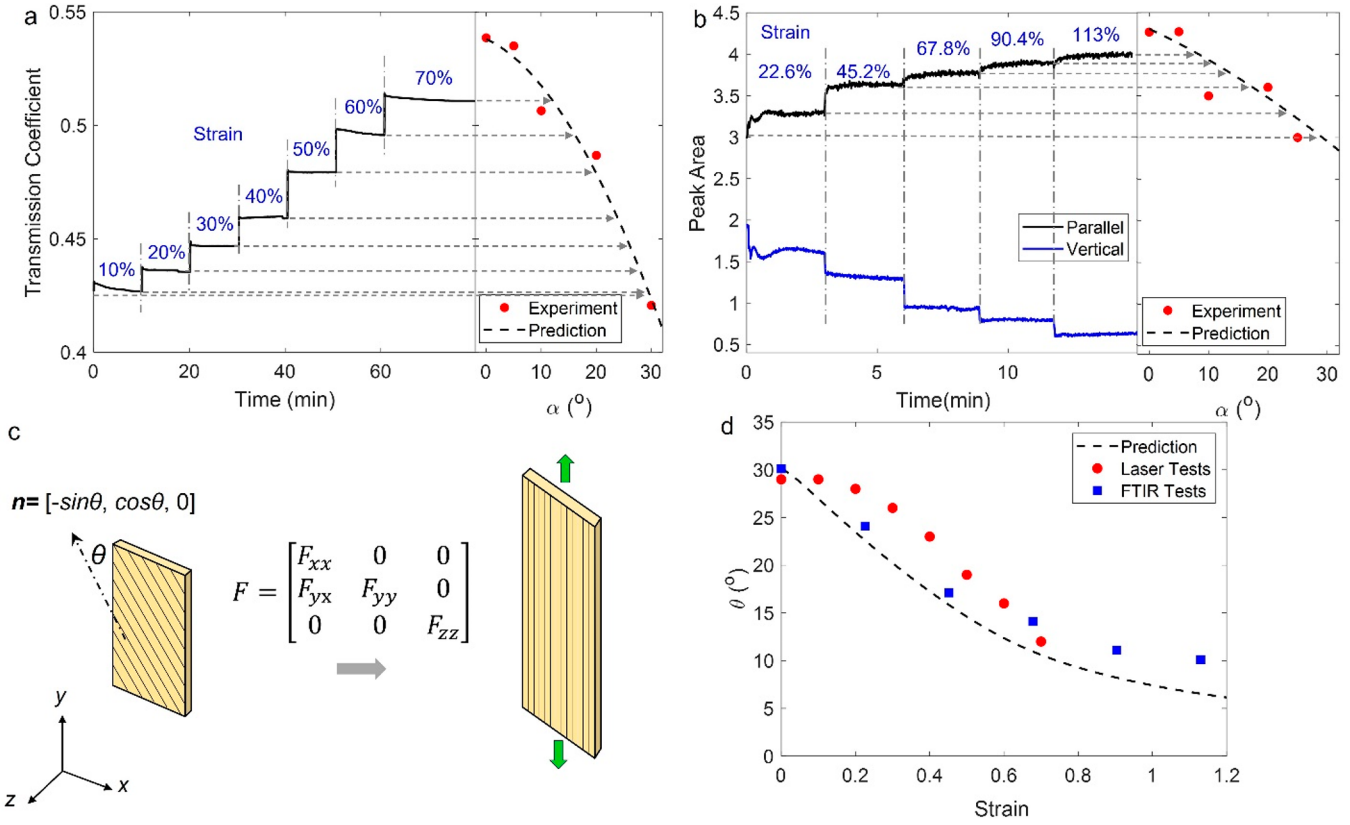

Figure 5. (a) Left: the evolution of transmission coefficient when the LCE sample is under the stepped loading condition. Right: the relationship between the transmission coefficient and the directional angle of mesogens. (b) Left: the evolution of absorption peak area in parallel and perpendicular directions when the LCE sample is under the stepped loading condition. Right: The relationship between the absorption peak area and the directional angle of mesogens. (c) Schematic view showing the modeling framework. (d) Evolution of the microscale direction of mesogens as a function of strain.

processes, which are plotted as solid curves in Figure 3d. The black curve in the figure represents the evolution of the order parameter when the LCE is strained at 1%/min (or 1.67×10^{-4} s^{-1}). Since the time scale of the loading event, 6000 s, is much higher than the highest relaxation time (220 s) identified in Figure 3b, it can be treated as the equilibrium evolution of the order parameter. With a higher loading rate, the increment of order parameter will be delayed due to the relaxation of mesogens, which can be predicted as

$$S(\varepsilon) = S(\varepsilon)|_{1\%/\min}[1 - e^{-\varepsilon/k\tau(\varepsilon)}] \quad (6)$$

where $S(\varepsilon)|_{1\%/\min}$ is the increment of order parameter at 1%/min, and k is the loading rate, and $\tau(\varepsilon)$ is the relaxation time described in eq 5. A simple derivation of eq 6 is included in the SI (Section S6).

In addition to the optical measurements shown in Figure 3d, the LCE sample was subject to FTIR measurements with 47%/min and 100%/min loading rates. The identified evolutions of order parameters are shown in the SI (Figure S7). The evolution of order parameter from optical measurements at 1%/min loading rate is mapped to the different loading rates using eqs 3 and 6 and presented in Figures 3d and S7 as dashed curves. Overall, the predictions in these two figures are seen to be very close to the experimental data, which proves the effectiveness of the developed method in characterizing the mesogen alignment degree of LCE networks with continuous loading conditions, as well as the determined relaxation time scales of mesogen order parameters.

The stress−strain relationship during the uniaxial tension of LCE samples were recorded and compared to the evolution of order parameters determined using the optical measurements (SI, Section S8). It is observed that at a given loading rate, the true stress first increases with the true strain at a near-constant rate, and then enters the soft-elasticity zone with a dramatically decreased curve slope. After reaching a critical strain, the polymer chains within the LCE networks approach their extensibility, and the stress starts to increase notably. One clear correlation between the stress−strain relationship and the evolution of the order parameter is that the critical strain for strain hardening is close to the strain when order parameters approach the maximum value, as is highlighted by gray arrows in the figure. Physically, this is when the polymer chains a maximally aligned, further increasing the strain changes the bond length which requires more stress input.

2.4. Mesogen Reorientation with Deformation in Monodomain LCE Networks. While previous sections focused on reorientation and rotation dynamics of polydomain LCE networks, here we examine the same dynamics of monodomain nematic LCEs. To characterize the time scale of the mesogen reorientation, a monodomain LCE sample was first prepared by stretching a polydomain LCE by 120%. The monodomain structure was then fixed by applying the UV light to generate a second interpenetrating network. Next, the LCE sample was cut and stretched to perform optical measurements, wherein the stretching direction was 30° with respect to the initial mesogen alignment direction (Figure 4a). During the tests, the polarization direction of the incident light was

https://doi.org/10.1021/acsami.1c20082
ACS Appl. Mater. Interfaces 2022, 14, 1961−1972

fixed along the tension direction. As the strain increased, the mesogens were expected to reorient themselves toward the tensile direction (Figure 4b). Note that the in-chain mesogens in the monodomain LCE have been highly aligned prior to the measurements, and the directional angle between the stretch and mesogen alignment (30°) is small. Therefore, the mesogens are expected to maintain their alignment degree, and gradually realign themselves to the tension direction.

In the first group of tests, the monodomain LCE sample was continuously stretched at different loading rates (1%/min, 50%/min, and 100%/min, respectively). After the strain reached 100%, the sample was stabilized for 17 min. The transmission coefficient evolution of the LCE network during the loading step is plotted in Figure 4c. It is observed that the transmitted light power increases with strain level, as the aligned mesogens in the monodomain LCE reorient to the same direction of polarized light. The increment tends to stabilize after reaching ∼80% strain, suggesting a saturated degree of mesogen reorientation. However, the difference in the transmission coefficient with different loading rates is less significant. The transmission coefficients of the monodomain LCE network during the stabilization period are plotted as a function of time in Figure 4d. They are seen to remain constant over the entire period, with negligible differences among different loading rates. The comparison in these two figures indicates that the time scale for the mesogen reorientation could be much lower compared to the loading rate adopted in the tests.

FTIR characterizations were performed on the same monodomain LCE sample to examine the mesogen reorientation kinetics with the deformation. The sample was stretched continuously at 20%/min, 100%/min, and 450%/min to 80% engineering strain, with the initial mesogen alignment direction 30° from the tension direction. After that, the LCE sample was stabilized for a few minutes. The absorption peaks of the C−S bond in these two loading steps were monitored in the parallel and perpendicular directions of tension, and the evolutions of peak areas are shown in Figure 4e,c, respectively. It is observed that during the tension step, the absorption peak area in the parallel direction increases as the mesogens reorient to the loading direction and decreases in the perpendicular direction. The peak areas are maintained during the stabilization step. The FTIR characterization results confirm that the reorientation rate of polymer chains within the monodomain LCE network is faster than the selected loading rates. Considering the highest loading rate of 450%/min (or 0.075 s^{-1}) in these tests, the time scale for the mesogen orientation is estimated to be below 13.3 s (1/0.075 s^{-1}).

In addition to revealing the short time scale of the mesogen reorientation, the optical and FTIR measurements, combined with theoretical modeling, are used to identify the relationship between the microscale directional angle of mesogens and the strain level of the monodomain LCE sample. The relationship is first experimentally determined. During the optical measurement, the monodomain LCE sample was stretched in a stepped manner the initial mesogen 30° from tension direction. The strain was increased by 10% each time, followed by 10 min of stabilization. The evolution of the transmission coefficient is shown in Figure 5a (left figure). On the other hand, the red dots on the right side of Figure 5a are the experimental data of transmission coefficients with different directional angles between light polarization and sample stretching. They are the same data points in Figure 1b. The dashed line represents the curve fitting using the nonlinear regression method discussed in Section 2.2. Note that the programming strain of the LCE sample in this section is the same as that studied in Section 2.1. For a specific strain level during the stepped loading process, the direction of microscale mesogens can be determined by looking into the directional angles on the right side of the figure at the equivalent value of the transmission coefficient. The identified directional angles at different strain levels are plotted in Figure 5d as circular red dots. It is seen that the angle decreases from 30° with the strain level. When the strain is 70%, the directional angle is ∼12°.

Polarized FTIR characterizations were performed on the same monodomain LCE sample with the same loading condition. The evolution of the absorption peak areas of the C−S bond is shown on the left side of Figure 5b. The peak area in the parallel direction of stretch increases with strain and decreases in the perpendicular direction. The red dots on the right side of Figure 5b are the experimental results of FTIR absorption peak areas with different direction angles of mesogens, which are the same data points presented in Figure 2d. The dashed line represents the curve fitting using the nonlinear regression method. After mapping between these two figures, the corresponding directional angle of mesogens are determined and plotted in Figure 5d as blue square dots.

Both optical and FTIR measurements show similar reorientation behaviors of the mesogen, despite that the decrease of directional angle in optical measurement is slower at the lower strain levels. The relationship can be further established from the theoretical point of view. Marner et al.[16] defined the well-known free energy function of the nematic LCE network. A unit vector $\boldsymbol{n}$ represents the direction of mesogens in the deformed configuration. For the 2D deformation, $\boldsymbol{n}$ is related to the directional angle of mesogens as Figure 5c. The order tensor of mesogens in the deformed configuration is $\boldsymbol{S} = S\,(\boldsymbol{n} \otimes \boldsymbol{n} - \boldsymbol{I}/3)$, and the anisotropic conformational tensor of the network is related to the order tensor as $\boldsymbol{A} = \boldsymbol{I} + 3\boldsymbol{S}$. In the reference configuration, the order tensor $\boldsymbol{S}_*$ and the conformational tensor $\boldsymbol{A}_*$ is defined in the same way based on the initial director $\boldsymbol{n}_*$. The neo-classical free energy follows:

$$\varphi = \frac{\mu}{2} tr(\boldsymbol{A}^{-1}\boldsymbol{F}\boldsymbol{A}_*\boldsymbol{F}^T) \tag{7}$$

where μ (1.1 MPa) is the network shear modulus, and $\boldsymbol{F}$ is the deformation gradient tensor.

Note that when the monodomain LCE sample is stretched in the oblique direction of the mesogen alignment and applied with the fixed boundary condition, the displacement field around the clamping area will be heterogeneous. A large LCE sample may also develop nonuniform deformation (e.g., shear banding) over the cross-section. Assessing how nonhomogenous motion influences optical and FTIR measurements deserves further investigation. In this paper, both experimental and theoretical studies on the mesogen reorientation are limited to the central part of the thin-film LCE sample where the motion is nearly uniform.

Following Cai and co-workers,[58] the deformation gradient tensor, projected onto a Cartesian frame with fixed basis vectors in Figure 5c, has components in matrix form as shown in the figure. With the network free energy defined in eq 7, the Piola−Kirchhoff engineering stress tensor may be calculated following standard arguments:[59]

https://doi.org/10.1021/acsami.1c20082
ACS Appl. Mater. Interfaces 2022, 14, 1961−1972

$$\boldsymbol{P} = \frac{\partial \varphi}{\partial \boldsymbol{F}} \tag{8}$$

The evolution of nematic order in the equilibrium state follows:

$$(\boldsymbol{I} - \boldsymbol{n} \otimes \boldsymbol{n})\frac{\partial \varphi}{\partial \boldsymbol{n}} = \boldsymbol{0} \tag{9}$$

With the prescribed boundary conditions that $F_{yy} = 1+\varepsilon$ and $P_{xx} = 0$, eqs 7−9 can be solved numerically to obtain the director $\boldsymbol{n}$, and thus the directional angle of mesogens as a function of engineering strain ε.

The theoretical prediction on the directional angle is shown in Figure 5d as the dashed curve. Overall, the experimental data and model predictions match each other closely, which suggests the effectiveness of the characterization and analysis using optical and FTIR measurements. The experimental data of the optical and FTIR measurements are slightly higher than the predictions from neo-classic network theory. This might result from two reasons: first, the neo-classic network theory predicts the mesogen alignment and reorientation of polymer melt under external loading, while the LCE samples used in this work have considerable cross-linking density. Based on the synthesis stoichiometry, the network cross-linking density is estimated to be 13 mol %; second, the monodomain LCE sample was prepared using the two-stage polymerization, namely the polydomain LCE was first stretched and then subject to the UV irradiation, wherein a second interpenetrating network was formed to fix the alignment polymer chains. Both the cross-linking effect and the second interpenetrating network within the monodomain LCE samples would restrict the reorientation of mesogens. Therefore, the evolution of mesogen directional angle is slower than the theoretical predictions.

3. CONCLUSIONS

In this paper, the real-time alignment and reorientation of mesogens in nematic LCEs are studied at different loading rates. The optical and FTIR measurements examine the mesogen alignment degree of polydomain LCEs at different strain levels. The evolution of mesogen direction is also characterized by stretching the monodomain LCEs in the oblique direction of mesogen alignment. This work has several major contributions. First, the correlation between the macroscopic optical measurements and the microscale FTIR analysis is established, which can be described using a simple yet effective mathematical function. Second, the time scale of the mesogen alignment is shown to decrease with the strain level of polydomain LCEs following an exponential function. The relationship is demonstrated to be effective in mapping the evolutions of mesogen alignment degree at different loading rates. Third, without involving the change of mesogen alignment degree, the time scale of the mesogen reorientation of monodomain LCEs is negligible for the loading rates adopted in this work (up to 450%/min). The relaxation time of mesogen reorientation is predicted to be lower than 13.3s at room temperature for the materials studied. The evolution of the mesogen direction during the mesogen reorientation can be well predicted using a concise modeling framework. Overall, this study provides an effective platform to characterize and predict the real-time alignment and reorientation of mesogens in LCEs, which is more accessible to other researchers. It unravels the evolution of microscale LCE networks at different loading rates, which will significantly advance the understanding of the material energy dissipation behaviors from both experimental and theoretical points of view, as well as to provide guidance to design dissipative LCE materials and components for future biomedical devices, tissue replacements, and protective equipment.

4. MATERIALS AND METHODS

4.1. Preparation of Polydomain and Monodomain LCEs. The LCE samples were synthesized via a thiol−acrylate Michael addition reaction.[60] It was prepared using the diacrylate mesogen, 1,4-Bis-[4-(3-acryloyloxypropyloxy) benzoyloxy]-2-methylbenzene (RM257), dithiol spacer 2,2-(ethylenedioxy) diethanethiol (EDDET), and tetra-thiol cross-linker pentaerythritol tetrakis (3-mercaptopropionate) (PETMP), photoinitiator (2-hydroxyethoxy)-2-methylpropiophenone (HHMP), and thermal catalyst dipropylamine (DPA). RM257 was purchased from Wilshire Technologies (Princeton, NJ, U.S.A.). All the rest chemicals were purchased from Sigma-Aldrich (St. Louis, MO, U.S.A.).

The chemical structures of major precursor for LCE synthesis are shown in the SI (Section S9). To prepare the polydomain LCEs, mesogen monomer RM257 (powder) was dissolved by adding 40 wt % of toluene and heating at 80 °C on a hot plate. After the solution was cooled to room temperature, thiol spacer EDDET and cross-linker PETMP were added to the solution with a weight ratio of 5:1. The mole amount of acrylate groups in RM 257 was 15 mol % more than the combined amount of thiol groups in EDDET and PETMP. 0.38 wt % of photoinitiator PPO was then dissolved into the solution to enable the second-stage photopolymerization reaction, followed by the vacuum for 30 s to remove the air bubbles. The solution was finally poured into a mold and placed in a vacuum chamber at 80 °C for 12 h to evaporate the toluene and polymerize the network.

Monodomain LCE samples were prepared by stretching the polydomain LCE by 120%. UV light was then applied to generate a second interpenetrating network. The strain was released after 15 min of UV exposure, and the monodomain LCE samples were created.

4.2. Polarized Optical Measurements. The optical properties of LCEs were tested using the visible red light with 650 nm wavelength. The light was generated by a red laser source (Hiletgo Inc., Shenzhen, China) with a maximum output power of 5 mW. The transmitted light power was measured using a laser sensor (Model PM16−120, Thorlabs, Newton, NJ) with a maximum data acquisition frequency of 10 Hz. The experiments were performed on an MTS tester to enable the tension of the LCE samples, wherein the distance between the laser source and the laser sensor was 47 cm. The distance between the laser source and the LCE sample was 38 cm.

4.3. Polarized FTIR Characterizations. Polarized Fourier Transform Infrared Spectrometry (FTIR) was used to evaluate the alignment degree and orientation of mesogens when the LCEs were being stretched. The FTIR characterizations were performed at room temperature on a Nicolet 6700 FTIR spectrometer (Thermo Scientific, Waltham, MA, U.S.A.) with a KRS-5 wire grid polarizer and a custom-built sample holder. The LCE sample with a dimension of 16.5 × 3.9 × 0.45 mm^3 was exposed to polarized infrared light. The FTIR traces were collected in different stretch directions by averaging 32 scans of the signal at a resolution of 2 cm^{-1}.

■ ASSOCIATED CONTENT

Supporting Information

The Supporting Information is available free of charge at https://pubs.acs.org/doi/10.1021/acsami.1c20082.

Transmission coefficients of control samples without mesogens, optical properties and mesogen alignment of thick polydomain LCE sample, FTIR characterizations and mesogen alignment of polydomain LCE sample with a low cross-linking density, evolution of the mesogen order parameter of polydomain LCE with stepped

https://doi.org/10.1021/acsami.1c20082
ACS Appl. Mater. Interfaces 2022, 14, 1961−1972

loading, determination of the relaxation time of order parameter at different strain levels, derivation of eq 6, comparison between the order parameters in optical and WAXS measurements, stress−strain relations and evolution of mesogen order parameter, and chemical structures of the precursor chemicals for LCE synthesis (PDF)

AUTHOR INFORMATION

Corresponding Authors

Kevin Long − *Materials and Failure Modeling Department, Sandia National Laboratories, Albuquerque, New Mexico 87123, United States*; Email: knlong@sandia.gov

Kai Yu − *Department of Mechanical Engineering, University of Colorado Denver, Denver, Colorado 80217, United States*; orcid.org/0000-0001-9067-1673; Email: kai.2.yu@ucdenver.edu

Authors

Chaoqian Luo − *Department of Mechanical Engineering, University of Colorado Denver, Denver, Colorado 80217, United States*

Christopher Chung − *Department of Mechanical Engineering, University of Colorado Denver, Denver, Colorado 80217, United States*

Christopher M. Yakacki − *Department of Mechanical Engineering, University of Colorado Denver, Denver, Colorado 80217, United States*

Complete contact information is available at: https://pubs.acs.org/10.1021/acsami.1c20082

Notes

The authors declare no competing financial interest.

ACKNOWLEDGMENTS

This work was supported by the Laboratory Directed Research and Development program at Sandia National Laboratories, a multimission laboratory managed and operated by National Technology and Engineering Solutions of Sandia, LLC, a wholly owned subsidiary of Honeywell International Inc. for the U.S. Department of Energy's National Nuclear Security Administration under contract DE-NA0003525. K.Y. acknowledges support from the National Science Foundation (CAREER Award CMMI-2046611). This paper describes objective technical results and analysis. Any subjective views or opinions that might be expressed in the paper do not necessarily represent the views of the U.S. Department of Energy or the United States Government. SAND2021-15896 J.

REFERENCES

(1) Clarke, S. M.; Tajbakhsh, A. R.; Terentjev, E. M.; Remillat, C.; Tomlinson, G. R.; House, J. R. Soft Elasticity and Mechanical Damping in Liquid Crystalline Elastomers. *J. Appl. Phys.* **2001**, *89*, 6530−6535.

(2) Traugutt, N. A.; Mistry, D.; Luo, C. Q.; Yu, K.; Ge, Q.; Yakacki, C. M. Liquid-Crystal-Elastomer-Based Dissipative Structures by Digital Light Processing 3d Printing. *Adv. Mater.* **2020**, *32*, 2000797.

(3) Luo, C.; Chung, C.; Traugutt, N. A.; Yakacki, C. M.; Long, K. N.; Yu, K. 3d Printing of Liquid Crystal Elastomer Foams for Enhanced Energy Dissipation under Mechanical Insult. *ACS Appl. Mater. Interfaces* **2021**, *13*, 12698−12708.

(4) Mistry, D.; Traugutt, N. A.; Yu, K.; Yakacki, C. M. Processing and Reprocessing Liquid Crystal Elastomer Actuators. *J. Appl. Phys.* **2021**, *129*, 130901.

(5) Mills, N. J.; Fitzgerald, C.; Gilchrist, A.; Verdejo, R. Polymer Foams for Personal Protection: Cushions, Shoes and Helmets. *Compos. Sci. Technol.* **2003**, *63*, 2389−2400.

(6) Viana, J. C. Polymeric Materials for Impact and Energy Dissipation. *Plast., Rubber Compos.* **2006**, *35*, 260−267.

(7) Viot, P. Polymer Foams to Optimize Passive Safety Structures in Helmets. *International Journal of Crashworthiness* **2007**, *12*, 299−310.

(8) Ula, S. W.; Traugutt, N. A.; Volpe, R. H.; Patel, R. R.; Yu, K.; Yakacki, C. M. Liquid Crystal Elastomers: An Introduction and Review of Emerging Technologies. *Liq. Cryst. Rev.* **2018**, *6*, 78−107.

(9) Wang, C. C.; Yang, K. C.; Lin, K. H.; Liu, H. C.; Lin, F. H. A Highly Organized Three-Dimensional Alginate Scaffold for Cartilage Tissue Engineering Prepared by Microfluidic Technology. *Biomaterials* **2011**, *32*, 7118−7126.

(10) Wicklein, B.; Kocjan, A.; Salazar-Alvarez, G.; Carosio, F.; Camino, G.; Antonietti, M.; Bergstrom, L. Thermally Insulating and Fire-Retardant Lightweight Anisotropic Foams Based on Nanocellulose and Graphene Oxide. *Nat. Nanotechnol.* **2015**, *10*, 277−283.

(11) Cox, S. C.; Thornby, J. A.; Gibbons, G. J.; Williams, M. A.; Mallick, K. K. 3d Printing of Porous Hydroxyapatite Scaffolds Intended for Use in Bone Tissue Engineering Applications. *Mater. Sci. Eng., C* **2015**, *47*, 237−247.

(12) Naebe, M.; Shirvanimoghaddam, K. Functionally Graded Materials: A Review of Fabrication and Properties. *Applied Materials Today* **2016**, *5*, 223−245.

(13) Davoodi, M. M.; Sapuan, S. M.; Yunus, R. Conceptual Design of a Polymer Composite Automotive Bumper Energy Absorber. *Mater. Eng.* **2008**, *29*, 1447−1452.

(14) Weiser, E. S.; Johnson, T. F.; St Clair, T. L.; Echigo, Y.; Kaneshiro, H.; Grimsley, B. W. Polyimide Foams for Aerospace Vehicles. *High Perform. Polym.* **2000**, *12*, 1−12.

(15) Ohm, C.; Brehmer, M.; Zentel, R. Liquid Crystalline Elastomers as Actuators and Sensors. *Adv. Mater.* **2010**, *22*, 3366−3387.

(16) Warner, M.; Terentjev, E. M. *Liquid Crystal Elastomers*; Oxford University Press: Oxford, 2003 1−354.

(17) Brommel, F.; Kramer, D.; Finkelmann, H. Preparation of Liquid Crystalline Elastomers. *Liquid Crystal Elastomers: Materials and Applications* **2012**, *250*, 1−48.

(18) Zentel, R. Liquid Crystalline Elastomers. *Angew. Chem.* **1989**, *101*, 1437−1445.

(19) Roach, D. J.; Yuan, C.; Kuang, X.; Li, V. C. F.; Blake, P.; Romero, M. L.; Hammel, I.; Yu, K.; Qi, H. J. Long Liquid Crystal Elastomer Fibers with Large Reversible Actuation Strains for Smart Textiles and Artificial Muscles. *ACS Appl. Mater. Interfaces* **2019**, *11*, 19514−19521.

(20) Li, Y.; Luo, C.; Yu, K.; Wang, X. Remotely Controlled, Reversible, on-Demand Assembly and Reconfiguration of 3d Mesostructures Via Liquid Crystal Elastomer Platforms. *ACS Appl. Mater. Interfaces* **2021**, *13*, 8929−8939.

(21) Li, Y.; Yu, H.; Yu, K.; Guo, X.; Wang, X. Reconfigurable Three-Dimensional Mesotructures of Spatially Programmed Liquid Crystal Elastomers and Their Ferromagnetic Composites. *Adv. Funct. Mater.* **2021**, *31*, 2100338.

(22) Yuan, C.; Roach, D. J.; Dunn, C. K.; Mu, Q. Y.; Kuang, X.; Yakacki, C. M.; Wang, T. J.; Yu, K.; Qi, H. J. 3d Printed Reversible Shape Changing Soft Actuators Assisted by Liquid Crystal Elastomers. *Soft Matter* **2017**, *13*, 5558−5568.

(23) Xie, P.; Zhang, R. Liquid Crystal Elastomers, Networks and Gels: Advanced Smart Materials. *J. Mater. Chem.* **2005**, *15*, 2529−2550.

(24) Urayama, K. Selected Issues in Liquid Crystal Elastomers and Gels. *Macromolecules* **2007**, *40*, 2277−2288.

(25) Merkel, D. R.; Shaha, R. K.; Yakacki, C. M.; Frick, C. P. Mechanical Energy Dissipation in Polydomain Nematic Liquid

Crystal Elastomers in Response to Oscillating Loading. *Polymer* **2019**, *166*, 148−154.
(26) Hotta, A.; Terentjev, E. M. Dynamic Soft Elasticity in Monodomain Nematic Elastomers. *Eur. Phys. J. E: Soft Matter Biol. Phys.* **2003**, *10*, 291−301.
(27) Hanzon, D. W.; Traugutt, N. A.; McBride, M. K.; Bowman, C. N.; Yakacki, C. M.; Yu, K. Adaptable Liquid Crystal Elastomers with Transesterification-Based Bond Exchange Reactions. *Soft Matter* **2018**, *14*, 951−960.
(28) Mistry, D.; Traugutt, N. A.; Sanborn, B.; Volpe, R. H.; Chatham, L.; Zhou, R.; Song, B.; Yu, K.; Long, K.; Yakacki, C. M. Soft Elasticity Optimises Dissipation in 3d-Printed Liquid Crystal Elastomers. *Nat. Commun.* **2021**, *12*, 6677.
(29) Traugutt, N.; Volpe, R.; Bollinger, M.; Saed, M. O.; Torbati, A.; Yu, K.; Dadivanyan, N.; Yakacki, C. Liquid-Crystal Order During Synthesis Affects Main-Chain Liquid-Crystal Elastomer Behavior. *Soft Matter* **2017**, *13*, 7013−7025.
(30) Saed, M. O.; Volpe, R. H.; Traugutt, N. A.; Visvanathan, R.; Clark, N. A.; Yakacki, C. M. High Strain Actuation Liquid Crystal Elastomers Via Modulation of Mesophase Structure. *Soft Matter* **2017**, *13*, 7537−7547.
(31) Saed, M. O.; Torbati, A. H.; Starr, C. A.; Visvanathan, R.; Clark, N. A.; Yakacki, C. M. Thiol-Acrylate Main-Chain Liquid-Crystalline Elastomers with Tunable Thermomechanical Properties and Actuation Strain. *J. Polym. Sci., Part B: Polym. Phys.* **2017**, *55*, 157−168.
(32) Murthy, N. S.; Minor, H. General Procedure for Evaluating Amorphous Scattering and Crystallinity from X-Ray Diffraction Scans of Semicrystalline Polymers. *Polymer* **1990**, *31*, 996−1002.
(33) Graewert, M. A.; Svergun, D. I. Impact and Progress in Small and Wide Angle X-Ray Scattering (Saxs and Waxs). *Curr. Opin. Struct. Biol.* **2013**, *23*, 748−754.
(34) Harada, M.; Ando, J.; Hattori, S.; Sakurai, S.; Sakamoto, N.; Yamasaki, T.; Masunaga, H.; Ochi, M. In-Situ Analysis of the Structural Formation Process of Liquid-Crystalline Epoxy Thermosets by Simultaneous Saxs/Waxs Measurements Using Synchrotron Radiation. *Polym. J.* **2013**, *45*, 43−49.
(35) Barnes, M.; Verduzco, R. Direct Shape Programming of Liquid Crystal Elastomers. *Soft Matter* **2019**, *15*, 870−879.
(36) Kotikian, A.; Truby, R. L.; Boley, J. W.; White, T. J.; Lewis, J. A. 3d Printing of Liquid Crystal Elastomeric Actuators with Spatially Programed Nematic Order. *Adv. Mater.* **2018**, *30*, 1706164.
(37) Thomsen, D. L.; Keller, P.; Naciri, J.; Pink, R.; Jeon, H.; Shenoy, D.; Ratna, B. R. Liquid Crystal Elastomers with Mechanical Properties of a Muscle. *Macromolecules* **2001**, *34*, 5868−5875.
(38) Anglaret, E.; Brunet, M.; Desbat, B.; Keller, P.; Buffeteau, T. Molecular Orientation in Liquid Crystal Elastomers. *Macromolecules* **2005**, *38*, 4799−4810.
(39) Aksenov, V.; Stannarius, R.; Tammer, M.; Kolsch, P.; Kremer, F.; Rossle, M.; Zentel, R. Ftir Spectroscopy of Smectic Elastomer Films under Lateral Strain. *Liq. Cryst.* **2007**, *34*, 87−94.
(40) Gharde, R. A.; Mani, S. A.; Jessy, P. J.; Amare, J. R.; Keller, P. Spectroscopic and Thermo-Mechanical Studies of Liquid Crystal Elastomer. *Key Eng. Mater.* **2015**, *659*, 495−499.
(41) Tammer, M.; Li, J.; Komp, A.; Finkelmann, H.; Kremer, F. Ftir-Spectroscopy on Segmental Reorientation of a Nematic Elastomer under External Mechanical Fields. *Macromol. Chem. Phys.* **2005**, *206*, 709−714.
(42) Bitri, N.; Gharbi, A.; Marcerou, J. P. Scanning Conoscopy Measurement of the Optical Properties of Chiral Smectic Liquid Crystals. *Phys. B* **2008**, *403*, 3921−3927.
(43) Cao, Z.; Xuan, L.; Hu, L.; Lu, X.; Mu, Q. Temperature Effect on the Diffraction Efficiency of the Liquid Crystal Spatial Light Modulator. *Opt. Commun.* **2006**, *267*, 69−73.
(44) Beica, T.; Moldovan, R.; Tintaru, M.; Enache, I.; Frunza, S. Measurements of Optical Anisotropy of a Calamitic Lyotropic Liquid Crystal. *Cryst. Res. Technol.* **2004**, *39*, 151−156.
(45) Benkelfat, B. E.; Horache, E. H.; Zou, Q.; Vinouze, B. An Electro-Optic Modulation Technique for Direct and Accurate Measurement of Birefringence. *Opt. Commun.* **2003**, *221*, 271−278.
(46) Yusuf, Y.; Sumisaki, Y.; Kai, S. Birefringence Measurement of Liquid Single Crystal Elastomer Swollen with Low Molecular Weight Liquid Crystal. *Chem. Phys. Lett.* **2003**, *382*, 198−202.
(47) El-Dessouki, T. A.; Roushdy, M.; Hendawy, N. I.; Naoum, M. M.; Zaki, A. A. Optical Measurements of Thermotropic Liquid Crystals. *J. Mod. Phys.* **2013**, *4*, 39−48.
(48) Swinehart, D. F. The Beer-Lambert Law. *J. Chem. Educ.* **1962**, *39*, 333.
(49) Kocsis, L.; Herman, P.; Eke, A. The Modified Beer-Lambert Law Revisited. *Phys. Med. Biol.* **2006**, *51*, N91.
(50) Ricci, R. W.; Ditzler, M.; Nestor, L. P. Discovering the Beer-Lambert Law. *J. Chem. Educ.* **1994**, *71*, 983.
(51) Born, M.; Wolf, E. *Principles of Optics: Electromagnetic Theory of Propagation, Interference and Diffraction of Light*; Elsevier: Amsterdam, 2013; pp 1−543.
(52) Shi, X.; Ge, Q.; Lu, H.; Yu, K. The Nonequilibrium Behaviors of Covalent Adaptable Network Polymers During the Topology Transition. *Soft Matter* **2021**, *17*, 2104−2119.
(53) Lei, M.; Yu, K.; Lu, H.; Qi, H. J. Influence of Structural Relaxation on Thermomechanical and Shape Memory Performances of Amorphous Polymers. *Polymer* **2017**, *109*, 216−228.
(54) Yu, K.; Ge, Q.; Qi, H. J. Reduced Time as a Unified Parameter Determining Fixity and Free Recovery of Shape Memory Polymers. *Nat. Commun.* **2014**, *5*, 1−9.
(55) Yu, K.; Xie, T.; Leng, J.; Ding, Y.; Qi, H. J. Mechanisms of Multi-Shape Memory Effects and Associated Energy Release in Shape Memory Polymers. *Soft Matter* **2012**, *8*, 5687−5695.
(56) Ge, Q.; Yu, K.; Ding, Y.; Qi, H. J. Prediction of Temperature-Dependent Free Recovery Behaviors of Amorphous Shape Memory Polymers. *Soft Matter* **2012**, *8*, 11098−11105.
(57) Yu, K.; McClung, A. J.; Tandon, G. P.; Baur, J. W.; Qi, H. J. A Thermomechanical Constitutive Model for an Epoxy Based Shape Memory Polymer and Its Parameter Identifications. *Mech. Time-Depend. Mater.* **2014**, *18*, 453−474.
(58) He, X.; Zheng, Y.; He, Q.; Cai, S. Uniaxial Tension of a Nematic Elastomer with Inclined Mesogens. *Extreme Mechanics Letters* **2020**, *40*, 100936.
(59) Holzapfel, G. A. *Nonlinear Solid Mechanics: A Continuum Approach for Engineering*; New York Wiley: Chichester, 2000; pp 1−392.
(60) Yakacki, C. M.; Saed, M.; Nair, D. P.; Gong, T.; Reed, S. M.; Bowman, C. N. Tailorable and Programmable Liquid-Crystalline Elastomers Using a Two-Stage Thiol- Acrylate Reaction. *RSC Adv.* **2015**, *5*, 18997−19001.

https://doi.org/10.1021/acsami.1c20082
ACS Appl. Mater. Interfaces 2022, 14, 1961−1972